Biochimica et Biophysica Acta 1848 (2015) 568–580

Contents lists available at ScienceDirect

Biochimica et Biophysica Acta

journal homepage: www.elsevier.com/locate/bbamem

Construction and validation of an atomic model for bacterial TSPO from electron microscopy density, evolutionary constraints, and biochemical and biophysical data

Konrad Hinsen [a,b], Aurore Vaitinadapoule [c,d,e,f,g,h], Mariano A. Ostuni [c,d,e,f], Catherine Etchebest [c,d,e,f,h], Jean-Jacques Lacapere [i,j,k,*]

[a] Centre de Biophysique Moléculaire (CNRS), Rue Charles Sadron, 45071 Orléans Cedex, France
[b] Synchrotron SOLEIL, Division Expériences, Saint Aubin, B.P. 48, 91192 Gif-sur-Yvette Cedex, France
[c] INSERM, UMR-S1134, 6 rue Alexandre Cabanel, Université Paris 7 Denis Diderot, F-75015 Paris, France
[d] Université Paris Diderot, Sorbonne Paris Cité, Paris, France
[e] Institut National de la Transfusion Sanguine (INTS), Paris, France
[f] GR-Ex, Laboratoire d'Excellence, Paris, France
[g] National Centre for Biological Sciences (NCBS), Tata Institute for Fundamental Research, GKVK Campus, Bangalore, Karnataka, India
[h] Dynamique des Structures et des Interactions des des Macromolécules Biologiques, France
[i] Sorbonne Universités, UPMC Univ Paris 06, Laboratoire de Biomolécules (LBM), 4 Place Jussieu, F-75005 Paris, France
[j] Ecole Normale Supérieure — PSL Research University, Département de Chimie, 24, rue Lhomond, 75005 Paris, France
[k] CNRS, UMR 7203 LBM, F-75005 Paris, France

ARTICLE INFO

Article history:
Received 1 August 2014
Received in revised form 1 October 2014
Accepted 20 October 2014
Available online 28 October 2014

Keywords:
Translocase 18 kDa
Membrane protein
Transporter

ABSTRACT

The 18 kDa protein TSPO is a highly conserved transmembrane protein found in bacteria, yeast, animals and plants. TSPO is involved in a wide range of physiological functions, among which the transport of several molecules. The atomic structure of monomeric ligand-bound mouse TSPO in detergent has been published recently. A previously published low-resolution structure of *Rhodobacter sphaeroides* TSPO, obtained from tubular crystals with lipids and observed in cryo-electron microscopy, revealed an oligomeric structure without any ligand. We analyze this electron microscopy density in view of available biochemical and biophysical data, building a matching atomic model for the monomer and then the entire crystal. We compare its intra- and intermolecular contacts with those predicted by amino acid covariation in TSPO proteins from evolutionary sequence analysis. The arrangement of the five transmembrane helices in a monomer of our model is different from that observed for the mouse TSPO. We analyze possible ligand binding sites for protoporphyrin, for the high-affinity ligand PK 11195, and for cholesterol in TSPO monomers and/or oligomers, and we discuss possible functional implications.

1. Introduction

Translocator protein (TSPO) is a transmembrane protein that is found from bacteria to mammals [1]. The mammalian form was first described in 1977 as a pharmacological target of benzodiazepine diazepam in the kidney [2], and thus named peripheral-type benzodiazepine receptor. It exhibits features distinct from the central nervous system benzodiazepine receptor $GABA_A$. Since its discovery, TSPO has been shown to be present in most tissues and primarily localized in the mitochondria. However, its function is not yet fully understood since it changes from bacteria to mammals [1]. It plays an important role in many mitochondrial functions from biogenesis to respiration and is involved in apoptosis [3]. In particular, TSPO participates in the transport of molecules across mitochondrial membranes, such as the import of cholesterol, which is the rate limiting step of steroid and bile salt synthesis [4]. In bacteria, TSPO has been shown to transport intermediates of the porphyrin biosynthesis pathway [5] and/or to catalyze the degradation of PPIX with the consumption of oxygen [6], as well as to regulate virulence activity [7].

Until recently, little was known about the three-dimensional structure of TSPO. First studies were designed to characterize transmembrane domains by a topological approach [8] that were later on shown to be alpha helices [9]. The first atomic structure of mouse TSPO was

* Corresponding author.
E-mail addresses: konrad.hinsen@cnrs-orleans.fr (K. Hinsen), aurore.vaitinadapoule@inserm.fr (A. Vaitinadapoule), mariano.ostuni@inserm.fr (M.A. Ostuni), catherine.etchebest@inserm.fr (C. Etchebest), jean-jacques.lacapere@upmc.fr (J.-J. Lacapere).

http://dx.doi.org/10.1016/j.bbamem.2014.10.028
0005-2736/

solved by NMR this year [10]. The free protein in detergent exhibits a highly flexible structure that could only be stabilized by a high-affinity drug ligand, PK 11195. In contrast, a previous low resolution three-dimensional structure of bacterial TSPO from *Rhodobacter sphaeroides* in lipids was obtained by cryo-electron microscopy (cryo-EM) of helical crystals in the absence of any ligand [11]. It reveals that monomers consisting of five transmembrane helices associate to form a homodimer with the dimer interface involving three helices of each monomer. However, helix–helix connectivity within a monomer was not analyzed by the authors. There have been various attempts to build atomic models to fit this cryo-EM density, either using Rosetta modeling [12], or by homology modeling based on the recently solved ligand-bound structure of the mouse orthologue [13]. The dimeric structure raises several questions about the functional unit and the transport mechanism. Another arrangement of TSPO has been proposed for the mouse orthologue from EM images, suggesting an association of three to four monomers [14,15].

In the present work, we build a *polymeric structure* for bacterial ligand-free TSPO in lipids based on the cryo-EM density 3D map (EMDB entry: 1698). We carefully analyze the densities, isolate monomers and individual transmembrane helices, characterize the connections between these helices, and build a complete model fitting the EM density [16,17]. We generate contact predictions using several programs and analyze the monomer as well as the polymeric association of TSPO observed in the crystal. We explore different transmembrane arrangements suggested by previously published models [12,13,18,19]. Finally, we use our model to analyze the ligand binding sites and possible transport mechanisms in line with available biochemical data [7,20–25].

2. Material and methods

2.1. Electron microscopy data

We use EMDB entry 1698 [11], which is an electron microscopy density map for a helicoidal crystal of TSPO from *R. sphaeroides*. The coordinates given in the text refer to the grid points of this density whose spacing is 1.2 Å. The origin of the coordinates is located in the center of the tube.

2.2. Visualization software

For visualizing the electron microscopy data and identifying the helices and their connectivity, we used version 1.7 of the molecular visualization software Chimera [26].

2.3. Coarse-grain molecular dynamics

A homology model of bacterial TSPO (referred as homol_b-TSPO in the following) was constructed using Modeller version 9.11 [27] with the first of models of the NMR structure as the template structure (PDB ID: 2MGY). The target–template alignment was based on the alignment given in Fig. 4. 100 models were generated and the model with the highest DOPE score was selected. Coarse-grained (CG) Molecular Dynamics (MD) simulations of homol_b-TSPO and mouse TSPO were performed in a lipid box. We followed the protocol for CG membrane protein simulations described in [28], using the Gromacs 4.5.6 package. The homol_b-TSPO was embedded in a POPC membrane, solvated, and neutralized by the addition of chloride counter ions. The Martini 2.2 force field [29] was used for the protein, the membrane and the solvent. The box size was fixed to 15 nm in all directions. For the bacterial (respectively mouse) sequence, the system included 699 (700) POPC molecules, 18,702 (18,674) water molecules of type W, and one chloride ion (4 chloride ions). As recommended [28], we replaced roughly 5% of the water molecules by 821 (900) freeze-type water molecules. The secondary structures were analyzed prior to the simulation with the DSSP software (version DsspCMBI) [30] and restrained during the simulations, as required for the Martini force field. The systems were first minimized for 200,000 steps using a steepest descent algorithm, and then equilibrated for 20 ns. The integration time step was fixed to 20 fs. For equilibration, the system was coupled to a Berendsen thermostat at $T = 310$ K with 4.0 ps coupling time, and to a semi-isotropic Berendsen barostat at 1 bar (coupling time 4.0 ps and compressibility, 1×10^{-5} bar^{-1}). A shift function was used for the non-bonded interactions. The cutoff distance was fixed to 1.2 nm and 0.9 nm for Coulomb and van der Waals interactions, respectively. The pair list was updated every 10 steps. The dielectric constant was set to 15. For the 1 μs production period, a V-rescale algorithm was used for the thermostat (1 ps coupling time) and a semi-isotropic Parrinello–Rahman barostat for the pressure (coupling time 12 ps and compressibility, 3×10^{-4} bar^{-1}).

Four protein structures were selected (every 200 ns) along the simulation and an all-atom model was constructed for each of them using a backward protocol recently developed by Tieleman's group [31]. The Amber force field was chosen for the reconstruction. The protocol parameters were the default ones.

2.4. Construction of the atomic model for TSPO

An initial ideal-helix structure was generated from the primary sequence using PyMOL [32]. The helix pairs TM2–TM3 and TM4–TM5, which have the shortest loops, were folded using Molecular Dynamics (MD) simulations performed with the Molecular Modeling Toolkit [33] using the Amber99-SB force field [34]. The system was simulated in vacuum. The simulation protocol starts with 50 steps of steepest-descent minimization. The subsequent MD runs use a Velocity-Verlet integrator, a time step of 1 fs, and distance constraints that keep all C_α–C_α distances in each of the two helices rigid. Atom velocities were initialized randomly from a Gaussian distribution corresponding to a temperature of 50 K, and 10,000 MD steps were performed for equilibration. After that, a harmonic distance restraint was added between the first and the last C_α atom in each two-helix domain. Its force constant was 200 kJ/mol, and the target distance varied from 4 nm initially to 1.5 nm by steps of −0.5 nm. Each time the target distance was changed, 5000 steps of MD were performed. The protocol was run several times with different initial velocities in order to obtain multiple structures from which we chose the one that best fitted the EM density.

The TM2–TM3 and TM4–TM5 assemblies thus generated and the unmodified TM1 structure were placed by hand into the EM density. The loops linking the helices were generated using Modeller version 9.10 [27]. The Molecular Modeling Toolkit was used again for constructing multimers using the symmetry of the helicoidal crystal, and for further refinement with respect to the electron density map. The refinement consisted of an annealing protocol based on MD runs in which the Amber99-SB force field was complemented with an energy term proportional to the EM density map, during which the crystal symmetry of the assembly was regularly enforced.

The orientation of the helices was compared to the predictions made using the LIPS method (LIPid-facing Surface) [35].

2.5. Evolutionary correlation detection methods

We used two multiple sequence alignments (MSA). The first one is the 917 sequence MSA that was used to establish the structural model of TSPO by Evfold [18], the only difference being that we moved the bacterial TSPO sequence to the top of the alignment. The second MSA, containing 600 sequences, was obtained using HMMer3 [36] with the bacterial TSPO sequence as a query. To identify co-evolution in TSPO, we tested five methods: CAPS [37,38], CMAT [39], PSICOV [40], MIBP [41], and Evfold [42]. Taken together, these

five methods generated around 45,000 pairs of residues. All the pairs were first filtered to account for the helical properties of the TMs and their relative orientation deduced from a crude 2D topology. Based on the location of the TM helices and the loops deduced from TM prediction (Fig. 4), we removed all coevolution pairs between amino acids within the same helix (intra-helix) or within the same loop (intra-loop). Moreover, the relative orientation of TM helix pairs from Ncap to Ccap (Fig. 5), i.e. TM1 antiparallel to TM2, TM2 antiparallel to TM3 etc., implies that some amino acids are far away, e.g., Ncap residues of TM1 with respect to Ncap residues of TM2. We assumed that these residues would not interact.

Hence, the filter consisted in considering two co-evolved residues n and p belonging to helices TM_a and TM_b, respectively:

For $n \in TM_a$ and $TM_a \in [i,j]$ and m_a middle of TM_a. For $m \in TM_b$ and $TM_b \in [k,l]$ and m_b the middle of TM_b.

If TM_a parallel to TM_b:

- If $(n \in [i, m_a[$ and $p \in]m_b, l])$ => rejected pair
- If $(n \in]m_a, i]$ and $p \in]m_b, l])$ => rejected pair
- If $(n = m_a$ and $(p \in [k, m_b - k]$ or $p \in [l - m_b, l]))$ => rejected pair
- If $(p = m_b$ and $(n \in [i, m_a - i]$ or $n \in [j - m_a, j]))$ => rejected pair
- Else accepted pair

If TM_a anti-parallel to TM_b:

- If $(n \in [i, m_a[$ and $p \in [k, m_b[)$ => rejected pair
- If $(n \in]m_a, j]$ and $p \in]m_b, l])$ => rejected pair
- If $(n = m_a$ and $(p \in [k, m_b - k]$ or $p \in [l - m_b, l]))$ => rejected pair
- If $(p = m_b$ and $(n \in [i, m_a - i]$ or $n \in [j - m_a, j]))$ => rejected pair
- Else accepted pair

2.6. Distances and scoring from coevolution methods

We compared our model constructed to fit the EM density to bacterial models generated by homology from the human TSPO models provided in the supplementary material of Hopf and collaborators [18]. We examined the correspondence between scoring values and distance distribution in the monomeric models.

In the bacterial models, we calculated the distances for all predicted coevolutionary pairs (8420 and 6435 for 600 and 917 sequences, respectively). Among these pairs, we selected those with C_α–C_α distances below 10.5 Å (623 and 607 for 600 and 917 sequences, respectively). We analyzed the EVFold scores of these pairs and found a weak correlation, with only 127 and 138 (for 600 and 917 sequence, respectively) predicted coevolutionary constraints being in the 10.5 Å range and having a high score (among the top 5000). For the bacterial model constructed from the EM density, we examined the same set of predicted coevolutionary pairs (8420 and 6435 for 600 and 917 sequences, respectively). We selected the pairs with C_α–C_α distances below 10.5 Å (701 and 792 for 600 and 917 sequences, respectively). Among them, the correlation between scores and distance distribution was also weak, with only 140 and 144 (for 600 and 917 sequence, respectively) predicted coevolutionary constraints having a high score. For all of the models described above, only 20% of the predicted pairs with the highest EVFold scores correspond to close contacts in the structure. Similar conclusions were obtained using the PSICOV method.

3. Results

3.1. Rigid fitting of atomic models into the EM density map

A first attempt at fitting atomic models into the EM density has been described in [12], using the two best-scoring models proposed by the

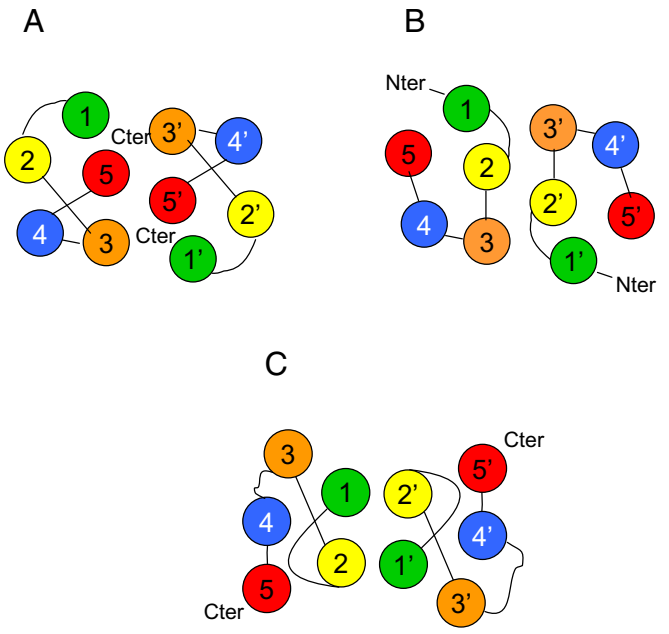

Fig. 1. Dimeric arrangements of the transmembrane helices in various bacterial TSPO models fitted into the cryo-EM density map. (A) and (B) Best ab-initio models (90–5 and 60–9, respectively) from Hopf and collaborators [18]. (C) Best homodimer model from Jaremko and collaborators [13] built using mouse TSPO atomic structure as a template.

Rosetta software. These two models respect the helix arrangements within the monomer and the dimer that were previously suggested in [11]. They differ from each other in having opposite orientations relative to the membrane plane (Fig. 1A and B) [12]. A second attempt to fit the EM density [13] assumed that the tertiary and quaternary structures of bacterial and mammalian TSPO are the same (Fig. 1C) and were built using the mouse TSPO atomic structure [10]. Several models were generated in this work, constructed as dimers using molecular modeling techniques, and then fitted rigidly into the EM density. The models differ in their dimer interfaces, the best one by the authors' criteria having a dimer interface consisting of two TMs. None of the models respects all the constraints of the EM density, which in particular indicates a dimeric interface made of three helices. The assembly of multiple dimers into a ring and the stacking of rings to form the tubular crystal is not reproduced either by these models.

We built a homology model for bacterial TSPO based on the NMR data [10] which we then placed into the crystal with TM3, TM4 and TM5 at the dimer interface. However, we were unable to place correctly all the TMs for mainly two reasons: (i) the compactness of the structure, which prevents a good simultaneous fit of all the TMs, and (ii) the location of TM1 in between TM2 and TM3 (Fig. 1C), which seems to prevent a correct positioning of these TMs because of the shortness of connection between TM2 and TM3 in bacteria. It has to be recalled that the NMR structure was solved in detergent with PK 11195, a high affinity ligand bound in a hydrophobic pocket in the middle of the five TMs, which stabilizes the structure. In the absence of a ligand, the TSPO structure is much more flexible [10,15]. We have performed coarse-grained molecular dynamics (CG-MD) in a lipid environment to check if protein flexibility could improve the fit to the EM density. After 1 μs the structure without ligand shows large movements of the TMs with the largest movement observed for TM1, but none of the selected conformations along the CG-MD simulation trajectory improves the quality of the fit into the EM density. We also performed CG-MD of the dimer in a lipid environment, with no better results. We thus started from the EM density to build a new atomic model, with the goal of respecting all the crystal constraints.

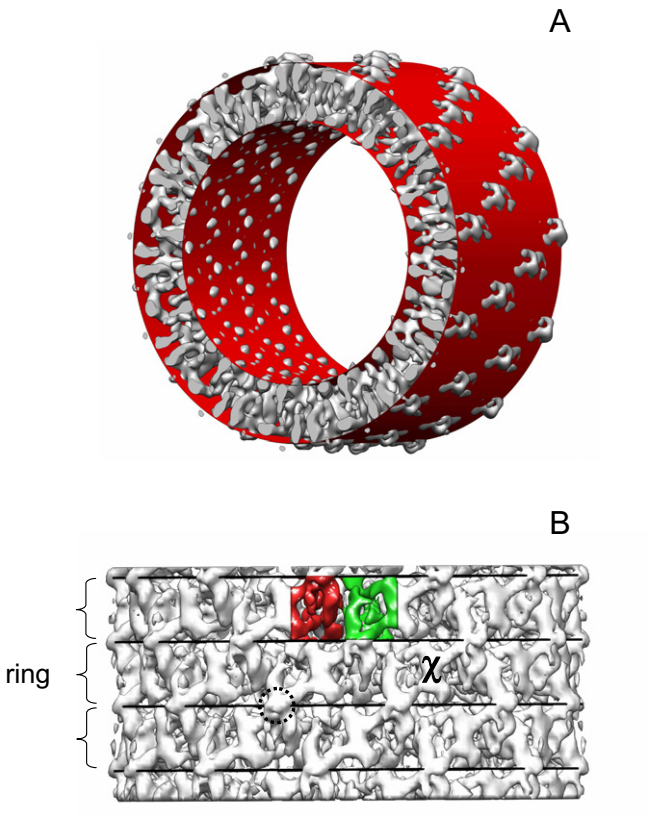

Fig. 2. Cryo-EM density map of bacterial TSPO at 2.0σ. (A) Side view showing the densities outside of the membrane. The two red cylinders correspond to the top and bottom of the membrane and are separated by 35 Å. (B) Top view showing the structure of the crystal as a stack of rings of dimers. The rings are separated by black lines. Two individual monomers are colored in red and green. Densities extruding from the membrane plane are labeled as χ symbol within a ring and as dotted circle between adjacent rings.

3.2. Interpretation of the EM density map

Fig. 2A shows the cryo-EM 3D density map for bacterial TSPO (EMDB entry: 1698), with the upper and lower limits of a membrane of 3.5 nm thickness indicated by red cylindrical surfaces. Few densities appear above and below the membrane. The cylinder is formed of stacked rings (Fig. 2B) containing twelve TSPO homo-dimers each [11]. Among the densities extruding from the membrane plane, some belong to the ring (χ symbol) but others join two adjacent rings (dotted circle). Two monomers have been selected in one of the rings for further analysis, and are shown colored in green and red (Fig. 2B).

Looking at planes parallel to the membrane in these two monomers (Fig. 3), we observe, as mentioned by Korkhov and collaborators [11], isolated densities that are easily attributed to transmembrane helices in the middle of the membrane (Fig. 3B). However, this attribution is more difficult when looking at planes above and below (Fig. 3A and C, respectively). We placed colored spheres (one color per helix) of corresponding size on each density in the central plane and checked continuity on the planes above and below to follow the connections needed to construct a 3D model (Fig. 3D).

In order to build an atomic model, we first analyzed the primary sequence alignments of bacterial and animal TSPO (Fig. 4) to locate the amino acid sequences of the individual transmembrane helices. Careful attention was given to residues usually placed at the membrane interface, such as tryptophan residues [43]. It has been verified previously from NMR data [9] that peptides corresponding to putative transmembrane helices of mouse TSPO were indeed structured into helices, an observation that was recently confirmed by the full atomic structure [10]. Connectivity between transmembrane helices in the densities has been assumed where spheres in one plane tend to overlap. Differences in the lengths of the loops, as well as for the N- and C-termini, have also been taken into account in our assessment of connectivity. Indeed, the C-terminus is longer than the N-terminus since it contains the polyhistidine tag [11]. The longest loop (loop 1) is located between the first (TM1) and the second (TM2) transmembrane helices and faces the cytosol, like the C-terminus. There is only one place in the density map that can accommodate this long loop between TM1 and TM2 (Fig. 5A): it corresponds to the largest density (χ symbol) that protrudes outside the tube (Fig. 2). The assignment of TM2 to the yellow spheres was motivated by the proximity between yellow and orange spheres (Fig. 5B), which is constrained by the very short loop (loop 2) between TM2 and TM3 (Fig. 4). The green spheres must then correspond to TM1, which is confirmed by the small density that protrudes inside the tube (Fig. 2) and that could match with the N-terminus. The assignment of the three first TMs is thus green, yellow and orange spheres for TM1, TM2 and TM3, respectively. The identification of the red spheres with TM5 is supported by the protruding density (dotted circle) on the outer surface of the tube (Fig. 5C), which could match the C-terminus polyhistidine tag, as previously suggested by Korkhov and collaborators [11]. This leaves the blue spheres as representing TM4, in agreement with the connectivity with the orange spheres (Fig. 5D) that matches loop 3 between TM3 and TM4. The final complete attribution (Fig. 5E) is green, yellow, orange, blue and red spheres for TM1, TM2, TM3, TM4 and TM5, respectively. We note that the geometrical arrangement of the five TMs in the density (Fig. 6A and B) resembles the description provided by Khorkov and collaborators [11].

3.3. Atomic model construction

As a first step in building an atomic model, we constructed a linear helix structure of bacterial TSPO from the sequence using the PyMOL program [32]. This structure is almost a single ideal helix, kinked only by some proline residues. We cut this linear structure into three domains TM1, TM2–TM3 and TM4–TM5, using the definition of the transmembrane domains shown by the boxes in Fig. 4. The reason for grouping TM2–TM3 and TM4–TM5 into two-helix domains is the shortness of the loops connecting these pairs, which imposes severe constraints on their relative position. The TM1 model has a bend at Pro 18 that corresponds well to a kink in the density. TM2–TM3 and TM4–TM5 were folded using Molecular Dynamics simulations with distance constraints on all pairs of alpha carbons within each transmembrane helix. With the constraints maintaining the geometry of the individual helices, the two-helix segments reliably fold into a compact structure in which the helices are nearly antiparallel. Multiple models were generated by starting the simulation with different randomly assigned initial velocities, leading to slightly different relative orientations of the helices. They were placed into the electron density map to select the best ones (Fig. 6A and B). The vertical placement of the TM helices was verified by looking at the residues located near the membrane interface. The orientations of the TM helices were validated by comparing their hydrophobic vectors to predictions of the lipid-facing surfaces made using the LIPS software [35]. For this step, sequences of two bacteria, two archaeabacteria and six animal species (including *R. sphaeroides* and mouse, respectively, for EM and NMR data) were aligned and the predicted transmembrane helices (shown as boxes in Fig. 4) were used as input for the LIPS server [44]. A helical wheel cartoon model shows the resulting orientations of the five transmembrane helices of TSPO (Fig. 6C). The orientation of TM1 in our model is not in agreement with the LIPS prediction but we gave higher priority to aligning the proline-induced bend in the constructed structure with the corresponding EM density. The orientation of the pair TM2–TM3 is in good agreement with the LIPS prediction. For the TM4–TM5 domain, the simulation protocol outlined above results in conformations that are credible in the monomer, but leads to clashes between helices belonging to neighboring monomers when placed into the crystal. We used the LIPS prediction to identify pairs of residues either

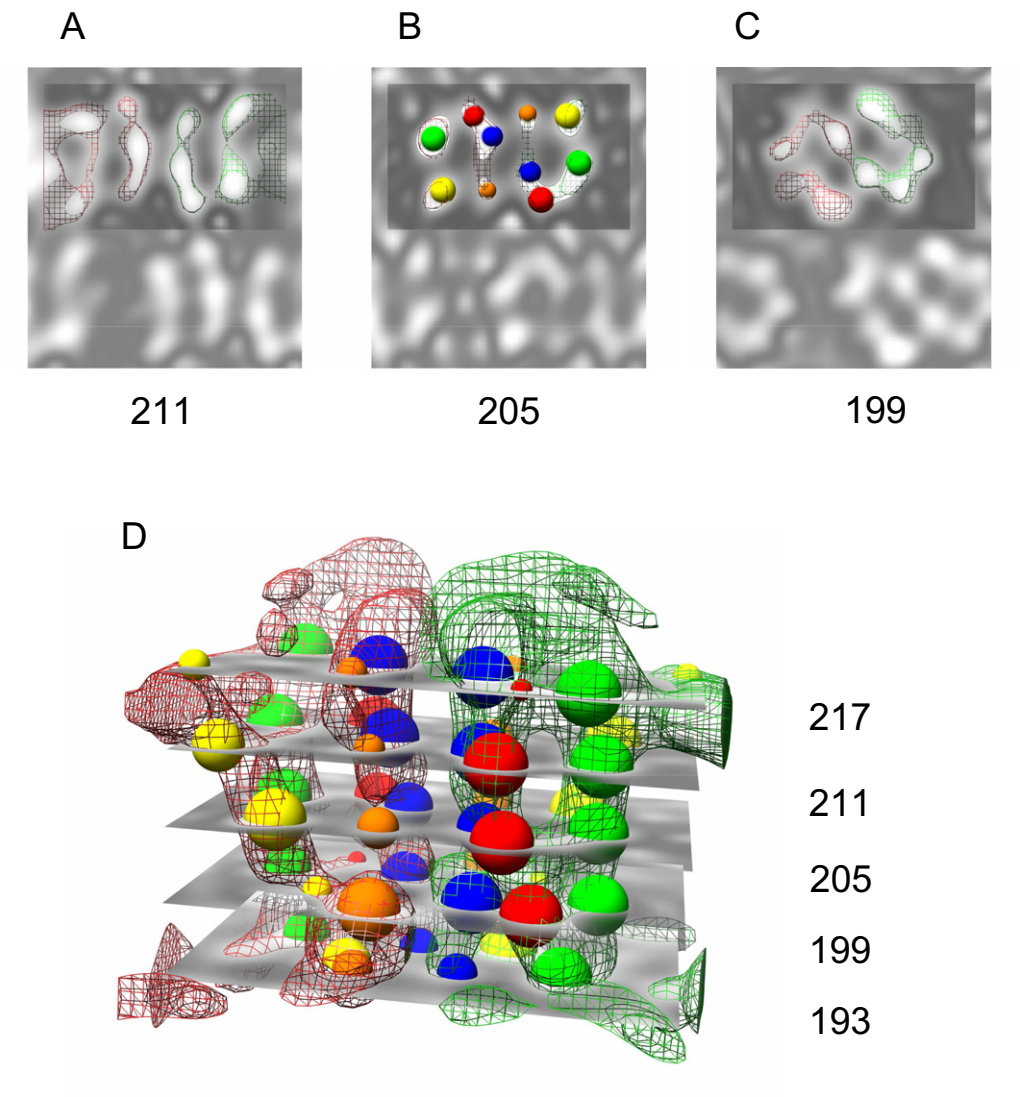

Fig. 3. Attribution of transmembrane helices. Planes of the cryo-EM density map of bacterial TSPO at 1.95σ, parallel to the membrane plane: (A) Upper plane (211) placed 7.2 Å above the middle of the membrane, (B) plane 205, corresponding to the middle of the membrane, (C) lower plane (199) placed 7.2 Å below the middle of the membrane. The darker boxes correspond to TSPO dimers. (D) Two adjacent densities forming a dimer (in red and green) with planes positioned at 5 levels (equally spaced at 7.2 Å and distributed from one side to the other of the membrane plane) have been used to place colored spheres and check continuities between planes.

facing each other at the interface (Val104/Thr140) or at the opposite face (Val106/Ala138) of the two helices, and put harmonic distance restraints on these pairs in order to get a structure compatible with both the LIPS prediction and the crystal geometry. This structure was further improved by a molecular dynamics run with added harmonic restraints that align the helix axes with the colored spheres from Fig. 3D. The final set of TM (1 to 5) was used to generate a full atomic model, including loops, using the Modeller software [27,45]. Modeller proposed several models, which were nearly identical in the helix regions but different in the loop arrangements. We chose the model whose loops were closest to the EM density map. The two longest loops (TM1–TM2 and TM3–TM4) were further optimized by a molecular dynamics run with added harmonic restraints that push the loops into positions more compatible with the EM map. The full TSPO monomer was then duplicated to fill the EM density with rings of dimers (Fig. 7A). A group of 8 monomers forming 4 dimers in 2 adjacent rings is shown in Fig. 7A. It was optimized in a subsequent step by a molecular dynamics run in which the EM density map was used as an external potential energy term, in order to generate a better positioning of the proteins within the density. Fine-tuning of the loops between the helices is difficult since the densities corresponding to these loops are not as well defined as the densities for the helices. Their volume probably arises from an average of conformations. The final model allows us to visualize contacts between the monomers within a ring (Fig. 7B) and also between rings (Fig. 7C).

3.4. Model validation by coevolution analysis

Amino acid covariation is becoming a powerful tool to predict 3D contacts within proteins and protein complexes [46]. It has been applied to predict structures of TSPO [18], which we have discussed above. We used coevolution results to assess our model rather than for guiding its construction. We compared the contacts predicted from coevolution analysis with the contacts observed in our EM-based model. We tested different prediction methods and two different sets of sequences (600-alignment and 917-alignment, see the Material and methods section). We measured intra- and intermolecular Cα–Cα distances between the different regions, i.e. TM, loops and N- and C-termini, and sorted them by ranges of distances (Table 1). When comparing intramolecular distances with predicted molecular contacts from evolutionary data, the best agreement (~94%) was obtained with the 600-sequence alignment. The main difference between the two alignments is small and was observed between TM–TM intramolecular regions. We conclude that the

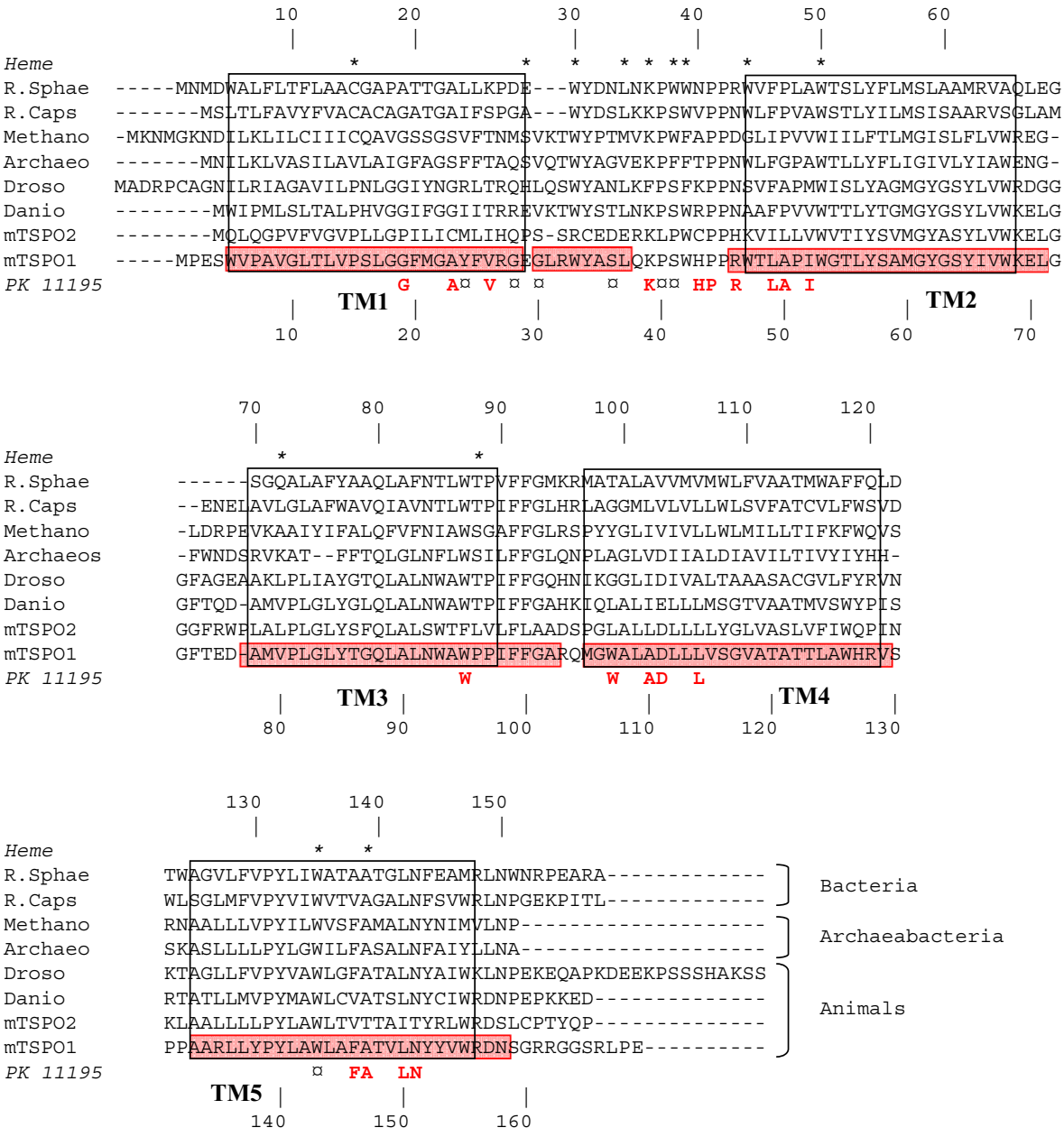

Fig. 4. Sequence and helix assignment of various TSPO homologues. Boxes depict the aligned amino acid sequences of the various species corresponding to the five predicted transmembrane domains (labeled TM1 to TM5). Red boxes on the mouse TSPO sequence correspond to helices in the atomic structure [13]. Numbers on top correspond to *Rhodobacter spaheroides* TSPO whereas numbers at the bottom correspond to mouse TSPO1. Amino acids mutated in the studies of heme binding [6,23], Ro5-4864 and PK 11195 [20,21] are indicated by stars in the top line and circled stars in the bottom line, respectively. Amino acids involved in PK 11195 binding in the atomic structure obtained from NMR data [10] are written in red bold characters in the bottom line. These residues have at least one atom at less than 3 Å from any atom of PK 111195.

atomic model of the monomer that we constructed to fit the EM density is globally in agreement with the evolutionary constraints.

When comparing intermolecular distances with predicted molecular contacts, the agreement is smaller: only ~30% of the TM–TM contacts are predicted. Evolutionary constraints give fewer intermolecular contacts than those observed in the crystal (342 versus 451 in Table 1). A mode detailed analysis shows that this difference concerns mainly the contacts predicted between loops and transmembrane helices. It has to be noted that the contacts between the loops connecting TM1 and TM2, which stabilize the crystalline dimer inside a ring, are not predicted, whereas contacts between dimers in two adjacent rings (monomers 0 and 4 in the diagram of Fig. 8) are predicted. Dimeric interactions inside a ring are predicted to occur through monomers 0 and 2, involving mostly TM–TM interactions. Taking into account the natural flexibility of loops and that some crystallographic constraints could not be connected to evolutionary constraints, we conclude that the crystal assembly that we constructed to fit the EM density is globally in agreement with intra- and intermolecular distances predicted by the evolutionary constraints.

4. Discussion

4.1. Comparison to earlier structure predictions

Several atomic models of TSPO have been published previously, constructed using various molecular modeling techniques: based on the apolipoprotein structure [19], from evolutionary constraints [18] for human TSPO, by ab initio modeling guided by the EM density [12], or by homology modeling of bacterial TSPO from mouse TSPO [13]. The

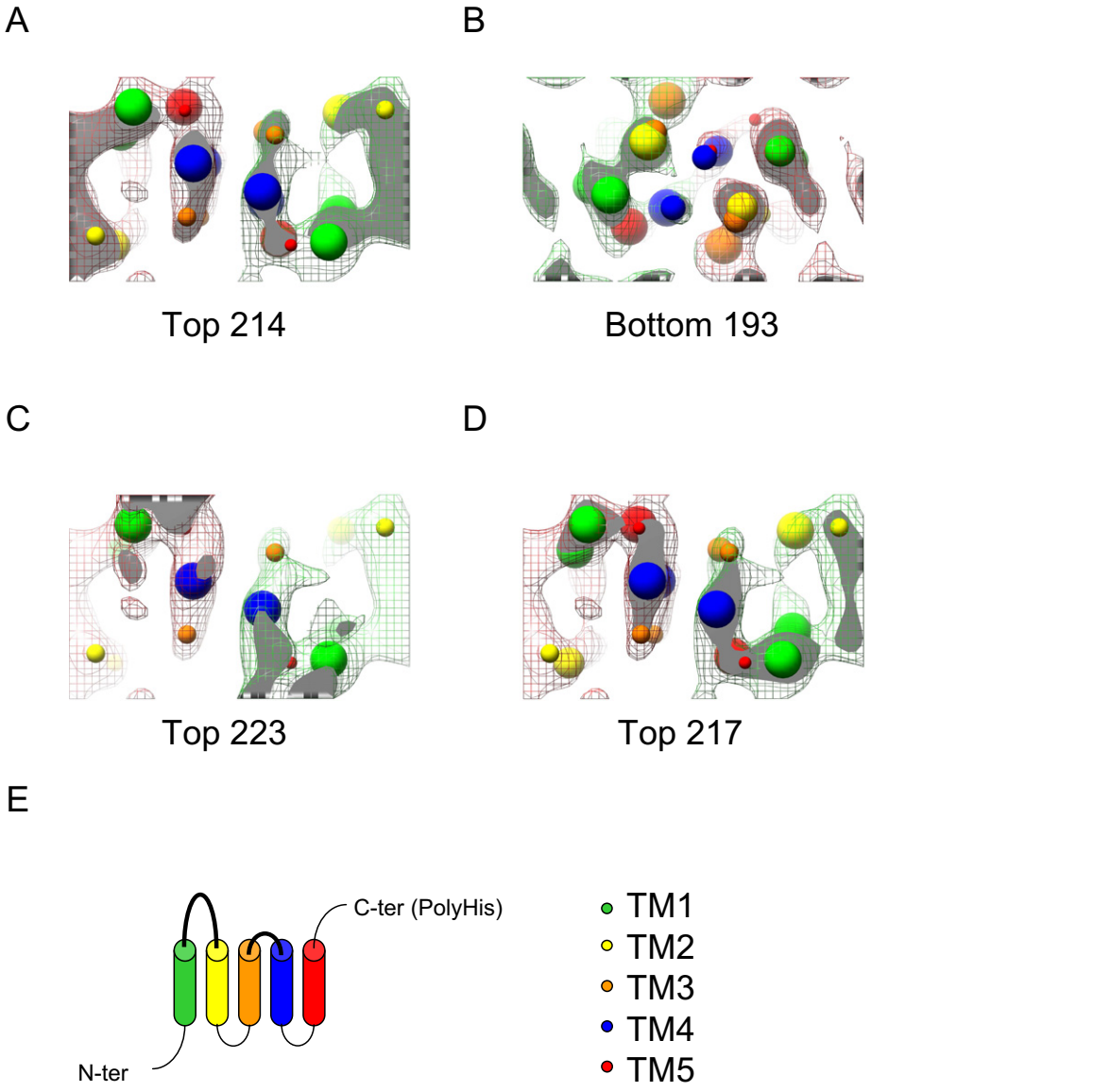

Fig. 5. Assignment of transmembrane helices. (A) Top view of plane 214 (10.8 Å above the middle of the membrane). The green-yellow connectivity shown in gray corresponds to loop 1. Note that the gray densities on the left and the right are not symmetrical due to the curvature of the tube. (B) Bottom view of plane 193 (14.4 Å below the middle of the membrane). The orange-yellow connectivity is shown by overlapping spheres. The gray density protruding from the green spheres corresponds to the N-terminus. (C) Top view of plane 223 (21.6 Å above the middle of the membrane). The gray density protruding from the red spheres corresponds to the C-terminus polyhistidine tag. (D) Top view of plane 217 (14.4 Å above the middle of the membrane). The orange-blue connectivity shown in gray corresponds to loop 3. (E) Colored TSPO model for the attribution of the 5 transmembrane helices.

transmembrane topologies of these models are quite different (Fig. 9). If we analyze the compatibility of these models with the EM density, the helix topology of apolipoprotein (Fig. 9A) involves loop crossings that seem incompatible with the EM density. Since no atomic model is available for comparison, we could not explore this further. Similarly, the topology of Hopf and collaborators' [18] model 90_5 (Fig. 9B) does not match the EM density map. In particular, the shortness of loop 2 (3 residues) is not compatible with the large distance between TM2 and TM3 that is required for fitting the EM density. In the second model (60_9) proposed by Hopf and collaborators [18], whose helix topology agrees with the NMR structure for mouse TSPO [10], the positions of TM2 and TM3 combined with the length of loop 2 are not compatible with the density map (Fig. 9C). Moreover, we could not find any EM density that could accommodate the N-terminus for this model's TM1 location.

There have been two attempts at constructing atomic models for bacterial TSPO that take into account the EM density. The models proposed by Li and collaborators [12] have very different TM topologies (non-sequential positioning of the TMs for the first model, and clockwise sequential positioning of the TMs for the second model). In their first model (Fig. 9D), TM5 is at the intra-ring dimer interface, and TM1 and TM2 are at the interface of dimers between rings. In their second model (Fig. 9E), the dimers are oriented upside down compared to their first model, with TM1 and TM2 located at the dimer interface and the long loop 1 facing the interior of the tube, where it does not fit into any EM density. In neither of these two models, the density extruding from the tube (Fig. 2A) contributes to any dimer interface. The dimer models proposed by Jaremko and collaborators [13] by homology modeling based on the mouse TSPO NMR structure [10] were constructed by placing two TMs at the dimer interface, in contradiction to the observation by Korkhov and collaborators [11] that the dimer interface is formed by three TMs. More generally, the automated procedures used for constructing the models discussed above seem to produce models that do not fit *all* the EM density for the 3D crystal. Our step-by-step manual approach, which takes the EM density as its starting point, leads to a more suitable model.

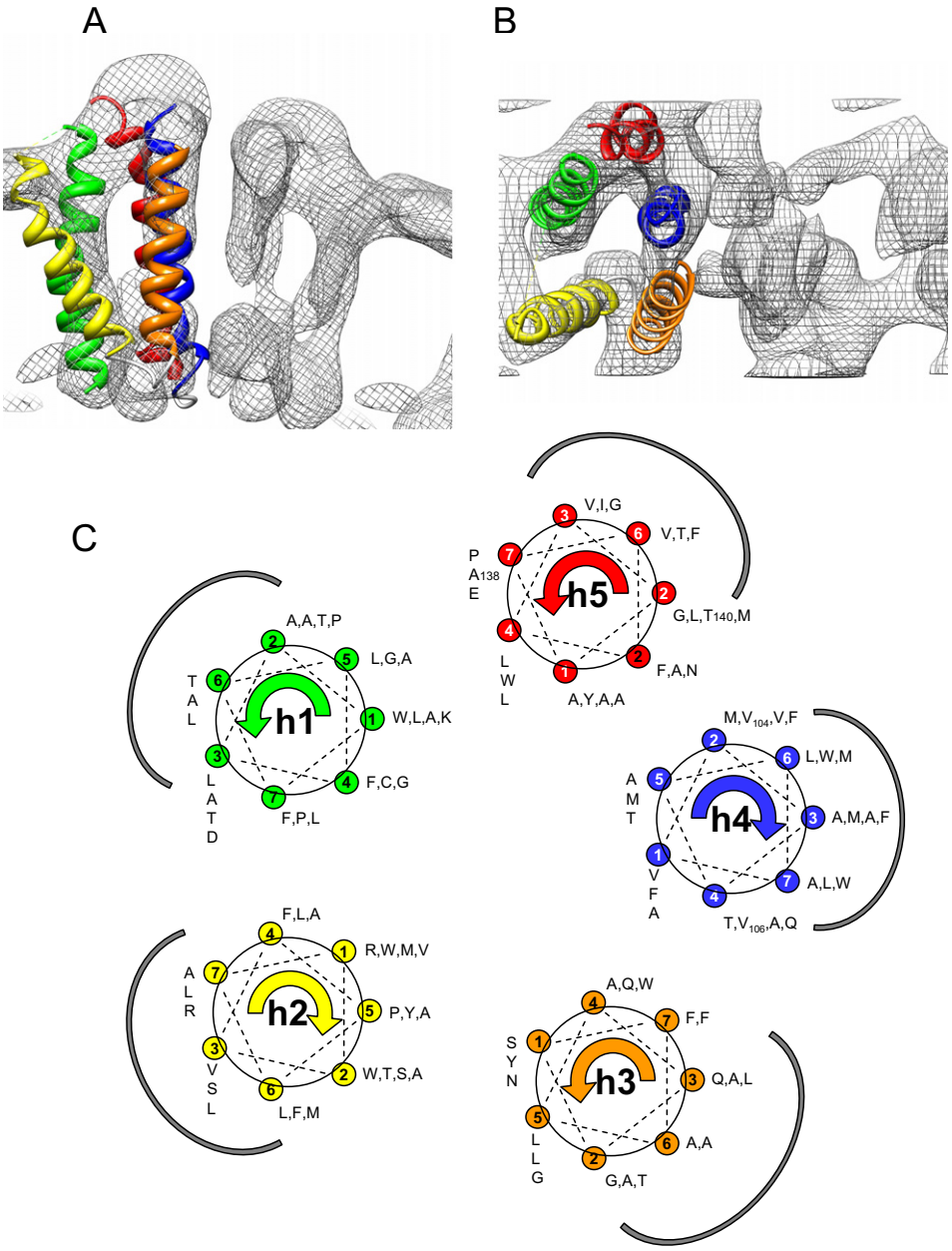

Fig. 6. Placement of the transmembrane helices into the TSPO density map. (A) Side and (B) top views of the bacterial TSPO helices placed into the cryo-EM density map. (C) Helical wheel cartoons illustrating the predicted lipid exposed faces (outlined with a gray line) of the five helices (H1 to H5) of the bacterial TSPO. The prediction was obtained by running the LIPS program on the aligned sequences of the various species shown in the boxes in Fig. 4.

Our unsuccessful attempt to build a homology model for bacterial TSPO based on NMR data [10] and to place it into the crystal with TM3 to TM5 at the dimer interface raises the question of the TM helix topology. The placement of TM1 and TM2 in sequential order with the other helices (Fig. 9F) leads to a much better fit into the EM density. Such a difference in helix topology can be due to a difference between bacteria and animals, in spite of a sequence identity between mouse and *R. sphaeroides* that is close to 30%. Indeed, the sequence alignment (Fig. 4) shows a gap between TM2 and TM3 for bacteria compared to animals. In line with this, it has to be noted that the amino acid sequence of TM1 is not well conserved during evolution. Moreover, bacteria have a membrane insertion different from mitochondria in that the first loop and the C-terminus face the cytosol rather than the matrix [7,23]. This may be due to the different location of DNA, which is in the cytosol of bacteria but in the nucleus of eukaryotic cells.

4.2. Analysis of oligomeric contacts in the crystal

The formation of crystals from membrane proteins requires not only correctly folded proteins with good intramolecular contacts, but also stabilization by intermolecular interactions. These interactions can take the form of TM contacts, but also take place between loops. The same contacts that stabilize the crystal could also contribute to oligomerization in the native membrane.

The present model allowed us to analyze bacterial TSPO crystals in more depth. It shows that the oligomeric packing of the proteins inside the 3D crystals carries valuable information about the different intermolecular interactions that could take place in vivo.

TSPO monomers interact by their large loop connecting TM1 and TM2, characterized by the large χ-shaped density observed outside the tubular crystal, which none of the previously proposed models can

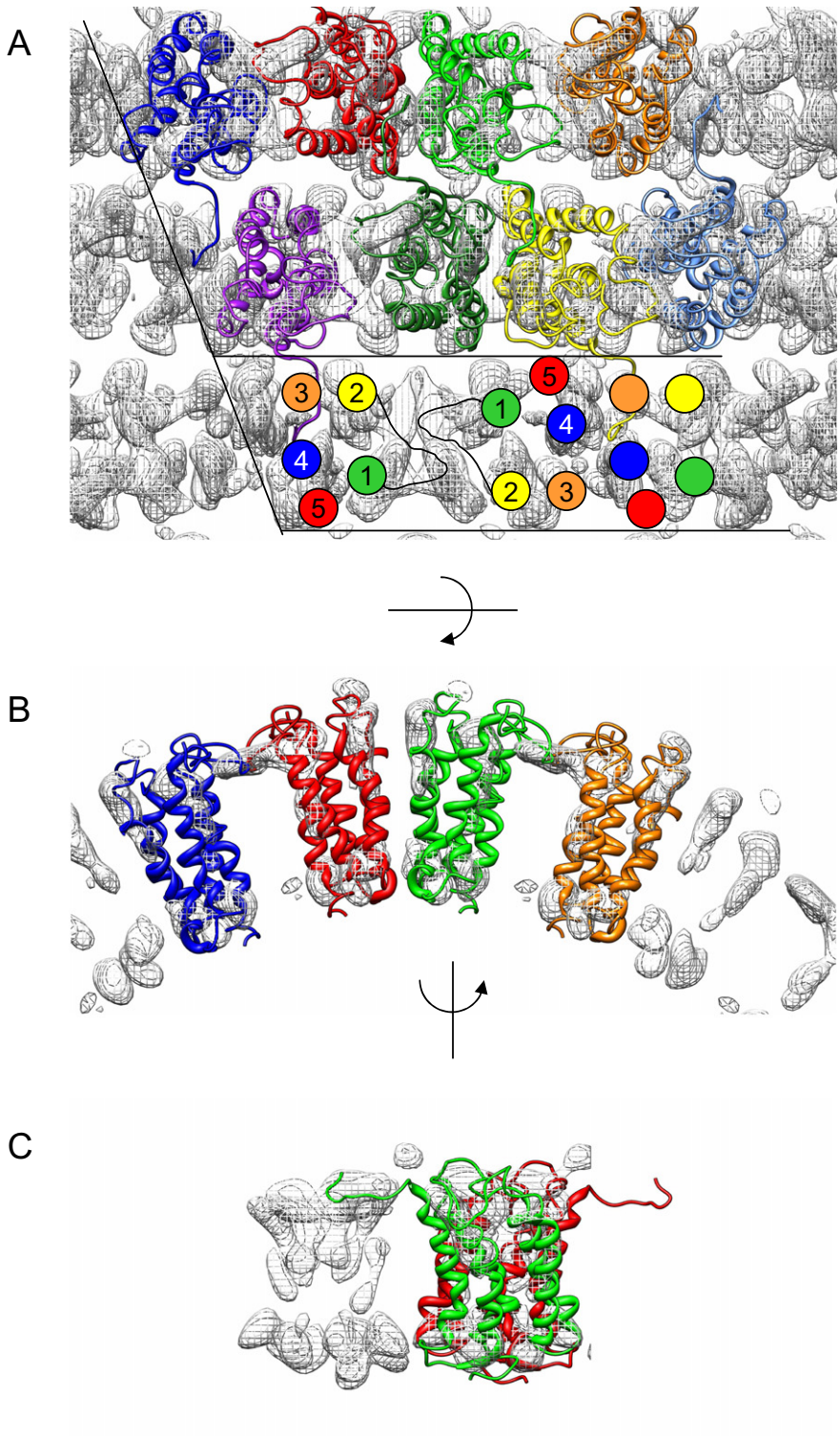

Fig. 7. Atomic model for bacterial TSPO in the cryo-EM density. (A) Top and (B) side views of monomers (colored individually) forming rings of dimers. (C) View between rings showing the C-terminus connecting the rings.

explain. The extended volume occupied by the two loops of two facing monomers suggests a high flexibility. This also means that our model is compatible with the formation of covalently bound dimers that are observed between mutated Trp38Cys [23] and which are located almost in the middle of the loop.

On the opposite side of the monomer, TM3, TM4 and TM5 interact with the same TM's of the adjacent monomer in a ring. The stabilization of two neighboring rings seems to involve the C-terminal domains of one monomer from each ring, characterized by a clear density protrusion observed at the ring interface. The interaction of two C termini containing the polyhistidine tag (His-Cter) could be favored by the presence of ions. Such a His-Cter_His-Cter stabilization could explain why a previous attempt to crystallize the recombinant mouse TSPO with the polyhistidine tag attached to the N-terminus did not succeed [14]. The His-Nter

Table 1
Cα–Cα distances between the different domains (TM, loops, N- and C-terminus) of our model fitted to the EM density. Non-TM means loops and terminal domains. "Model" means the total number of contacts in our atomic model, "917 and 600 seqs" refers to the contacts predicted from evolutionary constraints calculated with a set of different programs (see the Material and methods section). The intermolecular contacts are decomposed by pairs of monomers which are numbered as indicated in Fig. 8.

Distance (Å)			5.5	6.5	7.5	8.5	9.5	10.5	
Intra-molecular contacts	Model	TM–TM	23	58	108	195	339	507	843
		TM–nonTM	30	73	106	155	226	304	
		nonTM–nonTM	1	2	10	13	20	32	
	917 seqs	TM–TM	21	54	90	167	292	421	701
		TM–nonTM	24	64	94	133	196	259	
		nonTM–nonTM	1	1	7	9	13	21	
	600 seqs	TM–TM	23	57	102	182	318	457	792
		TM–nonTM	30	73	106	155	226	303	
		nonTM–nonTM	1	2	10	13	20	32	
Inter-molecular contacts	Models 0–1	TM–TM	0	0	0	0	0	0	176
	Models 0–2	TM–TM	0	4	9	28	50	97	
	Models 0–3	TM–TM	0	0	1	2	2	2	
	Models 0–4	TM–TM	3	9	17	22	44	73	
	Models 0–5	TM–TM	0	0	0	0	0	2	
	Models 0–6	TM–TM	0	0	1	2	2	2	
	Models 0–1	TM–nonTM	0	0	2	14	16	32	210
	Models 0–2	TM–nonTM	0	0	0	0	12	16	
	Models 0–3	TM–nonTM	0	2	6	12	21	33	
	Models 0–4	TM–nonTM	4	6	16	32	62	96	
	Models 0–5	TM–nonTM	0	0	0	0	0	0	
	Models 0–6	TM–nonTM	0	2	6	12	21	33	
	Models 0–1	nonTM–nonTM	0	1	4	12	18	26	65
	Models 0–2	nonTM–nonTM	0	0	0	2	4	7	
	Models 0–3	nonTM–nonTM	0	0	0	1	3	4	
	Models 0–4	nonTM–nonTM	0	0	4	14	16	24	
	Models 0–5	nonTM–nonTM	0	0	0	0	0	0	
	Models 0–6	nonTM–nonTM	0	0	0	1	3	4	
	600 seqs 0–1	TM–TM	0	0	0	0	0	0	96
	600 seqs 0–2	TM–TM	0	4	6	12	22	46	
	600 seqs 0–3	TM–TM	0	0	1	2	2	2	
	600 seqs 0–4	TM–TM	0	2	8	12	26	46	
	600 seqs 0–5	TM–TM	0	0	0	0	0	0	
	600 seqs 0–6	TM–TM	0	0	1	2	2	2	
	600 seqs 0–1	TM–nonTM	0	0	2	14	16	32	210
	600 seqs 0–2	TM–nonTM	0	0	0	0	12	16	
	600 seqs 0–3	TM–nonTM	0	2	6	12	21	33	
	600 seqs 0–4	TM–nonTM	4	6	16	32	62	96	
	600 seqs 0–5	TM–nonTM	0	0	0	0	0	0	
	600 seqs 0–6	TM–nonTM	0	2	6	12	21	33	
	600 seqs 0–1	nonTM–nonTM	0	0	0	0	0	0	36
	600 seqs 0–2	nonTM–nonTM	0	0	0	2	4	6	
	600 seqs 0–3	nonTM–nonTM	0	0	0	1	3	4	
	600 seqs 0–4	nonTM–nonTM	0	0	4	14	16	22	
	600 seqs 0–5	nonTM–nonTM	0	0	0	0	0	0	
	600 seqs 0–6	nonTM–nonTM	0	0	0	1	3	4	

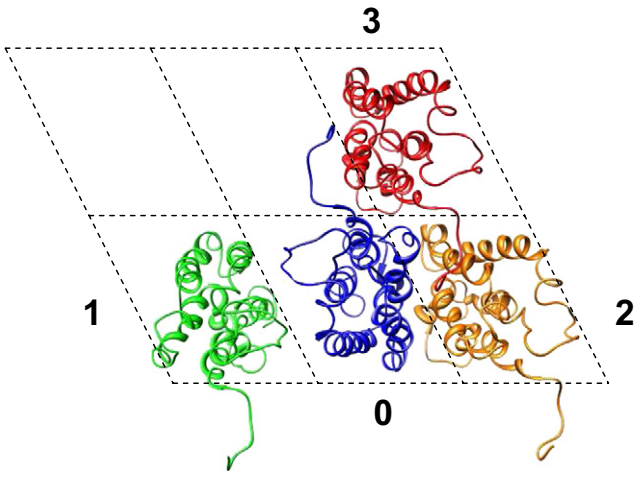

Fig. 8. Labeling of the TSPO monomer arrangement within the tubular crystal. The central monomer (0) is shown in blue, adjacent monomers within a row in green (1) and orange (2), and monomers from an adjacent ring in red (3).

insertion was governed by the observation that the mammalian C-terminus is involved in cholesterol binding [22,25].

4.3. Ligand binding sites and TSPO function

We used our atomic model of bacterial TSPO to explore the putative location of the ligand binding sites. The binding pocket for PK 11195 in mouse TSPO has been identified and involves amino acids of all the TMs and of the TM1–TM2 loop (Fig. 4). In our ligand-free model for bacterial TSPO, the five TMs can also form a pocket to bind PK 11195 since some of the corresponding bacterial residues are also oriented toward the center of the transmembrane domain. However, displacements of the helices and rotations around their axes are required for enabling close interaction with PK 11195. The TM1–TM2 loop that caps the PK 11195 in the mouse TSPO structure is outward-orientated, yielding access to the pocket (Fig. 10A). This suggests that this loop, which is involved in dimer interaction in bacteria, will have to move after the entry of PK 11195 into the pocket, or may serve as a guide toward the pocket for the ligand. Indeed, mutagenesis studies have shown that highly conserved amino acids present in this loop regulate PK 11195 affinity and selectivity [1,20–22,47]. Such a mechanism of ligand binding involves

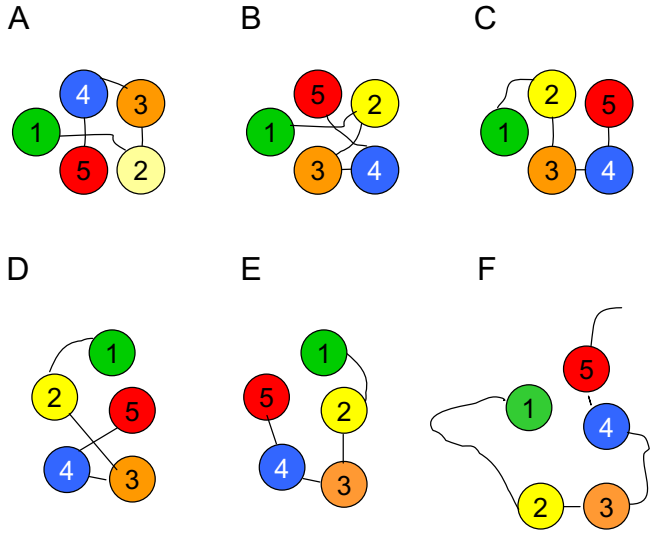

Fig. 9. Transmembrane helix arrangements in different models. (A) Homology model from Anzini and collaborators [19]. (B) and (C) Best ab initio models (90–5 and 60–9, respectively) from Hopf and collaborators [18]. (D) and (E) Ab initio model 1 and from Li and collaborators [12], respectively. (F) Our EM-based model.

a large rearrangement of the protein, which is in agreement with the conformational changes observed in CG-MD of mouse TSPO after removing the ligand. The difference in the amino acid sequence of this loop between bacterial and mammalian TSPO may contribute to the large observed change in PK 11195 affinity [48–50]. Point mutations in this loop as well as in the TMs forming the binding site would permit a better characterization of what makes the difference between bacteria and animals. In particular, amino acids involved in the PK 11195 binding pocket of the atomic structure of mouse TSPO that are not conserved in *R. sphaeroides* are good candidates.

Both porphyrins and PK 11195 have been described to bind to bacterial TSPO in a way similar to mammalian TSPO [23,48–53]. The bindings of porphyrins and PK 11195 are exclusive. It has also been shown that bacterial TSPO is involved in the efflux of porphyrin intermediates from the cell [53], suggesting that porphyrin may pass in between the transmembrane helices of TSPO. Two main hypotheses can be proposed: (i) Porphyrins and PK 11195 share the same binding site within the five TMs, and porphyrins are transported by the TSPO monomer. (ii) The binding sites are different but the presence of one ligand affects the binding site of the other (Fig. 10B). In the first case, the transport of porphyrins, which are larger molecules than PK 11195, could be accommodated by large amplitude fluctuations of the transmembrane domain of TSPO. Interestingly, the atomic model proposed here shows that Trp50 (TM2), which has been observed to be important for the binding of tetrapyrrols by bacterial TSPO [52], is located in between the five TM helices. Conversely, Trp135 (TM5) is facing outside the central cavity made by the TM helices, in agreement with the absence of effect upon its mutation [52]. However, we cannot exclude that porphyrins cross the membrane at the dimer interface as previously suggested [12]. In this second case, the involvement of the TM1–TM2 loop predicted to participate in the porphyrin binding site [23] would explain why PK 11195 cannot be bound at the same time. Indeed, the binding of porphyrin would prohibit the capping of the PK 11195 binding pocket. Porphyrin transport would thus occur in between dimers interacting by their loops rather than dimers interacting by their TM3 to TM5 as previously suggested [12]. The design of point mutations to test these different hypotheses for porphyrin transport is not an easy task. Aromatic residues in the putative channel formed by the five TM could be a first target. Aromatic residues present at the interface between dimers and in particular those of TM3 and TM4 placed at the bacterial TSPO interface could be a second one.

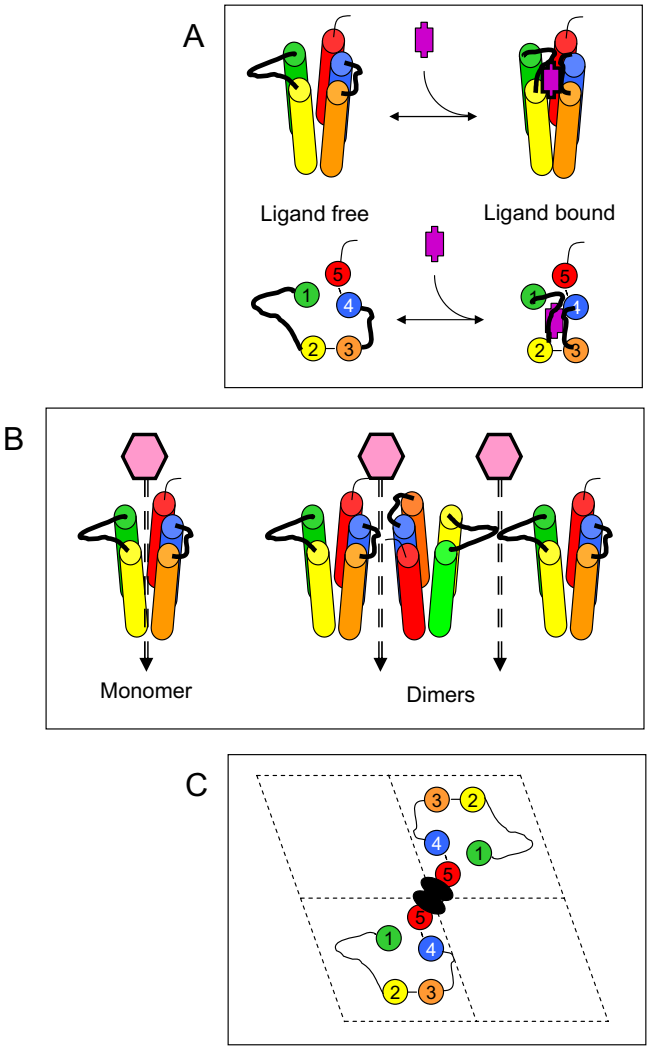

Fig. 10. Ligand binding sites of bacterial TSPO. (A) Putative PK 11195 binding mechanism in the atomic model for bacterial TSPO. Side views (upper panels) and top views (lower panel) of TSPO with PK 11195 shown in purple. (B) Putative porphyrin binding and transport (arrows) mechanism in the atomic model of bacterial TSPO. Side views of the monomer (left panel) and polymers (right panel) in a ring of TSPO monomers, with porphyrin shown as a purple hexagon. (C) Putative cholesterol-hopanoid binding site. Top view of the polymeric assembly of TSPO showing two individual monomers in two adjacent rings. Cholesterol or hopanoid molecules are shown as black ellipses at the interface of two monomers in the region of the C-terminal containing the CRAC (cholesterol recognition amino acid consensus) motif.

It has been suggested that bacterial TSPO may transport hopanoid [54] instead of cholesterol as in mammalian species [1]. Transport of cholesterol in animals clearly involves the CRAC domain (L/V/I-(X)1–5-Y-(X)1–5-R/K) located at the terminal part of TM5 [22,25]. Our atomic model suggests that this domain could face the lipid rather than the central region of the TSPO, in agreement with previous studies showing that mammalian TSPO could transport either membrane-resident cholesterol or cholesterol coming from external sources [55,56]. Our model also shows that this motif is located at the interface of two rings in the crystal, which is stabilized by C-terminus interactions [11]. Such dimer interactions, different from the intra-ring dimers mentioned previously for porphyrins, raise the question of cholesterol–hopanoid transport. The TSPO-cholesterol stoichiometry has been previously determined to be one to one [57–59]. One may thus suggest that two cholesterol molecules are face to face in between the dimer as previously described [60]. The cholesterol pathway through the membrane remains to be determined; it might involve protein–protein interfaces [55,61] or the central region of TSPO. Whatever the mechanism, the

two sites for cholesterol and the activating ligand are structurally distinct, since the binding of one does not preclude the binding of the other [22,25].

In conclusion, we propose a model for bacterial TSPO in a lipid crystal environment that shows a different topology than that observed for ligand-bound mouse TSPO in detergent, and also different oligomeric contacts compared to previously proposed models. Importantly, this model satisfies all the crystallographic constraints. Interestingly, the monomer is compatible with the high flexibility of the protein, as evidenced by NMR data [9,10]. It may suggest significant conformational changes that could occur during the PK 11195 binding due to transmembrane rearrangement and the flexibility of the long connecting loop between TM1 and TM2. The oligomers within and between rings give clues to understand the binding and transport of prophyrin and cholesterol.

Acknowledgments

This work was supported by the French National Center for Scientific Research (CNRS), the French National Institute for Health and Medical Research (INSERM), the French Ministry of Research (Universités Pierre et Marie Curie, et Denis Diderot-Paris 7), and the Regional Council of Reunion Island (No DIRED 20121417).

Appendix A. Supplementary data

Supplementary data to this article can be found online at http://dx.doi.org/10.1016/j.bbamem.2014.10.028.

References

[1] J. Fan, P. Lindemann, M.G. Feuilloley, V. Papadopoulos, Structural and functional evolution of the translocator protein (18 kDa), Curr. Mol. Med. 12 (4) (2012) 369–386.
[2] C. Braestrup, R.F. Squires, Specific benzodiazepine receptors in rat brain characterized by high-affinity (3H)diazepam binding, Proc. Natl. Acad. Sci. U. S. A. 74 (9) (1977) 3805–3809.
[3] V. Papadopoulos, M. Baraldi, T.R. Guilarte, T.B. Knudsen, J.-J. Lacapère, P. Lindemann, M.D. Norenberg, D. Nutt, A. Weizman, M.-R. Zhang, M. Gavish, Translocator protein (18 kDa): new nomenclature for the peripheral-type benzodiazepine receptor based on its structure and molecular function, Trends Pharmacol. Sci. 27 (8) (2006) 402–409.
[4] J.-J. Lacapère, V. Papadopoulos, Peripheral-type benzodiazepine receptor: structure and function of a cholesterol-binding protein in steroid and bile acid biosynthesis, Steroids 68 (7–8) (2003) 569–585.
[5] X. Zeng, S. Kaplan, TspO as a modulator of the repressor/antirepressor (PpsR/AppA) regulatory system in *Rhodobacter sphaeroides* 2.4.1, J. Bacteriol. 183 (21) (2001) 6355–6364.
[6] C. Ginter, I. Kiburu, O. Boudker, Chemical catalysis by the translocator protein (18 kDa), Biochemistry 52 (21) (2013) 3609–3611.
[7] A. Chapalain, S. Chevalier, N. Orange, L. Murillo, V. Papadopoulos, M.G. Feuilloley, Bacterial ortholog of mammalian translocator protein (TSPO) with virulence regulating activity, PLoS One 4 (6) (2009) e6096.
[8] E. Joseph-Liauzun, P. Delmas, D. Shire, P. Ferrara, Topological analysis of the peripheral benzodiazepine receptor in yeast mitochondrial membranes supports a five-transmembrane structure, J. Biol. Chem. 273 (4) (1998) 2146–2152.
[9] S. Murail, J.C. Robert, Y.M. Coïc, J.M. Neumann, M.A. Ostuni, Z.X. Yao, V. Papadopoulos, N. Jamin, J.-J. Lacapere, Secondary and tertiary structures of the transmembrane domains of the translocator protein TSPO determined by NMR. Stabilization of the TSPO tertiary fold upon ligand binding, Biochim. Biophys. Acta 1778 (6) (2008) 1375–1381.
[10] L. Jaremko, M. Jaremko, K. Giller, S. Becker, M. Zweckstetter, Structure of the mitochondrial translocator protein in complex with a diagnostic ligand, Science 343 (6177) (2014) 1363–1366.
[11] V.M. Korkhov, C. Sachse, J.M. Short, C.G. Tate, Three-dimensional structure of TspO by electron cryomicroscopy of helical crystals, Structure 18 (2010) 677–687.
[12] F. Li, Y. Xia, J. Meiler, S. Ferguson-Miller, Characterization and modelling of the oligomeric state and ligand binding behavior of the purified translocator protein 18 kDa from *Rhodobacter sphaeroides*, Biochemistry 52 (2013) 5884–5899.
[13] L. Jaremko, M. Jaremko, K. Giller, S. Becker, M. Zweckstetter, Toward the functional oligomerization state of tryptophan-rich sensory proteins, Protein Sci. 23 (8) (2014) 1154–1160.
[14] D. Teboul, S. Beaufils, J.-C. Taveau, S. Iatmanen-Harbi, A. Renault, C. Venien-Bryan, V. Vie, J.-J. Lacapere, Mouse TSPO in a lipid environment interacting with a functionalized monolayer, Biochim. Biophys. Acta 1818 (11) (2012) 2791–2800.
[15] J.-J. Lacapere, S. Iatmanen-Harbi, L. Senicourt, O. Lequin, P. Tekely, R.N. Purusottam, P. Hellwig, S. Krigel, S. Ravaud, C. Juillan-Binard, E. Pebay-Peyroula, V. Papadopoulos, Structural studies of TSPO, a mitochondrial membrane protein, in: I Mus Vetaux (Ed.), Membrane Protein Production for Structural Analysis, Springer, 2014, pp. 393–421 (Chapter 14).
[16] K. Hinsen, N. Reuter, J. Navaza, D.L. Stokes, J.-J. Lacapere, Normal mode-based fitting of atomic structure into electron density maps: application to sarcoplasmic reticulum Ca-ATPase, Biophys. J. 88 (2) (2005) 818–827.
[17] K. Hinsen, E. Beaumont, B. Fournier, J.-J. Lacapère, From electron microscopy maps to atomic structures using normal mode-based fitting, Methods Mol. Biol. 654 (2010) 237–258.
[18] T.A. Hopf, L.J. Colwell, R. Sheridan, B. Rost, C. Sander, D.S. Marks, Three-dimensional structures of membrane proteins from genomic sequencing, Cell 149 (2012) 1607–1621.
[19] M. Anzini, A. Cappelli, S. Vomero, M. Seeber, M.C. Menziani, T. Langer, B. Hagen, C. Manzoni, J.-J. Bourguignon, Mapping and fitting the peripheral benzodiazepine receptor binding site by carboxamide derivatives. Comparison of different approaches to quantitative ligand-receptor interaction modeling, J. Med. Chem. 44 (2001) 1134–1150.
[20] R. Farges, E. Joseph-Liauzun, D. Shire, D. Caput, G. Le Fur, G. Loison, P. Ferrara, Molecular basis for the different binding properties of benzodiazepines to human and bovine peripheral-type benzodiazepine receptors, FEBS Lett. 335 (1993) 305–308.
[21] R. Farges, E. Joseph-Liauzun, D. Shire, D. Caput, G. Le Fur, P. Ferrara, Site-directed mutagenesis of the peripheral benzodiazepine receptor: identification of amino acids implicated in the binding site of Ro5-4864, Mol. Pharmacol. 46 (1994) (1994) 1160–1167.
[22] H. Li, V. Papadopoulos, Peripheral-type benzodiazepine receptor function in cholesterol transport. Identification of a putative cholesterol recognition/interaction amino acid sequence and consensus pattern, Endocrinology 139 (1998) 4991–4997.
[23] A.A. Yeliseev, S. Kaplan, TspO of *Rhodobacter sphaeroides*. A structural and functional model for the mammalian peripheral benzodiazepine receptor, J. Biol. Chem. 275 (8) (2000) 5657–5667.
[24] F. Delavoie, H. Li, M. Hardwick, J.C. Robert, C. Giatzakis, G. Peranzi, Z.X. Yao, J. Maccario, J.-J. Lacapere, V. Papadopoulos, In vivo and in vitro peripheral-type benzodiazepine receptor polymerization: functional significance in drug ligand and cholesterol binding, Biochemistry 42 (15) (2003) 4506–4519.
[25] N. Jamin, J.M. Neumann, M.A. Ostuni, T.K.N. Vu, Z.X. Yao, S. Murail, J.C. Robert, C. Giatzakis, V. Papadopoulos, J.-J. Lacapere, Characterization of the cholesterol recognition amino acid consensus sequence of the peripheral-type benzodiazepine receptor, Mol. Endocrinol. 19 (3) (2005) 588–594.
[26] E.F. Pettersen, T.D. Goddard, C.C. Huang, G.S. Couch, D.M. Greenblatt, E.C. Meng, T.E. Ferrin, UCSF chimera — a visualization system for exploratory research and analysis, J. Comput. Chem. 25 (2004) 1605–1612.
[27] A. Sali, T.L. Blundell, Comparative protein modeling by satisfaction of spatial restraints, J. Mol. Biol. 234 (1993) 779–815.
[28] J. Barnoud, L. Monticelli, Coarse-grained force fields for molecular simulations, in: A. Kukol (Ed.), Molecular Modeling of Proteins, Series Methods Mol. Biol., 1215, 2014, p. 430.
[29] L. Monticelli, S.K. Kandasamy, X. Periole, R.G. Larson, D.P. Tieleman, S.-J. Marrink, The MARTINI coarse-grained force field: extension to proteins, J. Chem. Theory Comput. 4 (2008) 819–834.
[30] W. Kabsch, C. Sander, Dictionary of protein secondary structure: pattern recognition of hydrogen-bonded and geometrical features, Biopolymers 22 (12) (1983) 2577–2637.
[31] T.A. Wassenaar, K. Pluhackova, R. Böckmann, S.J. Marrink, D.P. Tieleman, Going backward: a flexible geometric approach to reverse transformation from coarse grained to atomistic models, J. Chem. Theory Comput. 10 (2) (2014) 676–690.
[32] The PyMOL Molecular Graphics System, Version 1.2, DeLano Scientific LLC, 2009.
[33] K. Hinsen, The molecular modeling toolkit: a new approach to molecular simulations, J. Comput. Chem. 21 (2) (2000) 79–85.
[34] V. Hornak, R. Abel, A. Okur, B. Strockbine, A. Roitberg, C. Simmerling, Comparison of multiple Amber force fields and development of improved protein backbone parameters, Proteins Struct. Funct. Genet. 3 (2006) 712–725.
[35] L. Adamian, J. Liang, Prediction of transmembrane helix orientation in polytopic membrane proteins, BMC Struct. Biol. 6 (2006) 13.
[36] S.R. Eddy, A probabilistic model of local sequence alignment that simplifies statistical significance estimation, PLoS Comput. Biol. 4 (5) (2008) e1000069.
[37] M.A. Fares, D. McNally, CAPS: coevolution analysis using protein sequences, Bioinformatics 22 (2006) 2821–2822.
[38] J. Segura, B. Oliva, N. Fernandez-Fuentes, CAPS-DB: a structural classification of helix-capping motifs, Nucleic Acids Res. 40 (Database issue) (2012) D479–D485.
[39] C.S. Jeong, D. Kim, Reliable and robust detection of coevolving protein residues, Protein Eng. Des. Sel. 25 (11) (2012) 705–713.
[40] D.T. Jones, D.W. Buchan, D. Cozzetto, M. Pontil, PSICOV: precise structural contact prediction using sparse inverse covariance estimation on large multiple sequence alignments, Bioinformatics 28 (2) (2012) 184–190.
[41] H. Gao, Y. Dou, J. Yang, J. Wang, New methods to measure residues coevolution in proteins, BMC Bioinforma. 26 (12) (2011) 206.
[42] D.S. Marks, L.J. Colwell, R. Sheridan, T.A. Hopf, A. Pagnani, R. Zecchina, C. Sanders, Protein 3D structure computed from evolutionary sequence variation, PLoS One 6 (12) (2011) e28766.
[43] M.R.R. De Planque, B.B. Bonev, J.A.A. Demmers, D.V. Greathouse, R.E. Koeppe II, F. Separovic, A. Watts, J.A. Killian, Interfacial anchor properties of tryptophan residues in transmembrane peptides can dominate over hydrophobic matching effects of peptide-lipids interactions, Biochemistry 42 (2003) 5341–5348.
[44] http://tanto.bioengr.uic.edu/lips/.
[45] http://www.salilab.org/modeller/.
[46] D. de Juan, F. Pazos, A. Valencia, Emerging methods in protein co-evolution, Nat. Rev. Genet. 14 (2013) 249–261.

[47] J. Fan, M.B. Rone, V. Papadopoulos, Translocator protein 2 is involved in cholesterol redistribution during erythropoiesis, J. Biol. Chem. 284 (44) (2009) 30484–30487.
[48] A.A. Yeliseev, K.E. Krueger, S. Kaplan, A mammalian mitochondrial drug receptor functions as a bacterial "oxygen" sensor, Proc. Natl. Acad. Sci. U. S. A. 94 (1997) 5101–5106.
[49] M. Gavish, I. Bachman, R. Shoukrun, Y. Katz, L. Veenman, G. Weisinger, A. Weizman, Enigma of the peripheral benzodiazepine receptor, Pharmacol. Rev. 51 (4) (1999) 629–650.
[50] G. Wendler, P. Lindemann, J.-J. Lacapère, V. Papadopoulos, Protoporphyrin IX binding and transport by recombinant mouse PBR, Biochem. Biophys. Res. Commun. 311 (4) (2003) 847–852.
[51] A.A. Yeliseev, S. Kaplan, A sensory transducer homologous to the mammalian peripheral-type benzodiazepine receptor regulates photosynthesis membrane complex formation in *Rhodobacter sphaeroides* 2.4.1, J. Biol. Chem. 270 (36) (1995) 21167–21175.
[52] A.A. Yeliseev, S. Kaplan, A novel mechanism for the regulation of photosynthesis gen expression by the TspO outer membrane protein of *Rhodobacter sphaeroides* 2.4.1, J. Biol. Chem. 274 (30) (1999) 21234–21243.
[53] S. Taketani, H. Kohno, T. Furukawa, R. Tokunaga, Involvement of peripheral-type benzodiazepine receptors in the intracellular transport of hem and porphyrins, J. Biochem. 117 (1995) 875–880.
[54] T. Rezanka, L. Siristova, K. Melzoch, K. Sigler, Hopanoids in bacteria and cyanobacteria — their role in cellular biochemistry and physiology, analysis and occurrence, Mini. Rev. Org. Chem. 7 (2010) 300–313.
[55] M.B. Rone, A.S. Midzak, L. Issop, G. Rammouz, S. Jagannathan, J. Fan, X. Ye, J. Blonder, T. Veenstra, V. Papadopoulos, Identification of a dynamic mitochondrial protein complex driving cholesterol import, trafficking, and metabolism to steroid hormones, Mol. Endocrinol. 26 (11) (2012) 1868–1882.
[56] K.E. Krueger, V. Papadopoulos, Peripheral-type benzodiazepine receptors mediate translocation of cholesterol from outer to inner mitochondrial membranes in adrenocortical cells, J. Biol. Chem. 265 (25) (1990) 15015–15022.
[57] J.-J. Lacapere, F. Delavoie, H. Li, G. Péranzi, J. Maccario, V. Papadopoulos, B. Vidic, Structural and functional study of reconstituted peripheral benzodiazepine receptor, Biochem. Biophys. Res. Commun. 284 (2) (2001) 536–541.
[58] M.A. Ostuni, O.R. Tumilasci, G. Péranzi, E.M. Cardoso, L.N. Contreras, A.L. Arregger, V. Papadopoulos, J.-J. Lacapere, Effect of translocator protein (18 kDa)-ligand binding on neurotransmitter-induced salivary secretion in rat submandibular glands, Biol. Cell. 100 (7) (2008) 427–439.
[59] M.A. Ostuni, G. Péranzi, R.A. Ducroc, M. Fasseu, B. Vidic, J. Dumont, V. Papadopoulos, J.-J. Lacapere, Distribution, pharmacological characterization and function of the 18 kDa translocator protein in rat small intestine, Biol. Cell. 101 (10) (2009) 573–586.
[60] J. Fantini, F.J. Barrantes, How cholesterol interacts with membrane proteins: an exploration of cholesterol-binding sites including CRAC, CARC, and tilted domains, Front. Physiol. 4 (2013) 31.
[61] L. Issop, M.B. Rone, V. Papadopoulos, Organelle plasticity and interactions in cholesterol transport and steroid biosynthesis, Mol. Cell. Endocrinol. 371 (1–2) (2012) 34–46.